3D particle models for composite laminates with anisotropic elasticity

Lei Wan[a], Dongmin Yang[a,*], Yaser Ismail[b], Yong Sheng[a]

[a] *School of Civil Engineering, University of Leeds, Leeds LS2 9JT, UK*
[b] *Independent Researcher, 31 Woodlea Mount, Leeds LS11 7NT, UK*

Abstract

This paper presents an assessment of three different particle based approaches for 3D modelling of fibre reinforced polymer (FRP) composite laminates with anisotropic elasticity, namely 3D Discrete Lattice model, 3D Hexagonal Close Packing model and Extended 2D Hexagonal and Square Packing model. These approaches are compared and evaluated against experimental results using a 0° ply lamina case. It has been confirmed that the Extended 2D Hexagonal and Square modelling approach in Discrete Element Method (DEM) is capable of modelling 3D composite laminates with better efficiency. Angle-ply lamina and two different laminates are modelled with the chosen particle approach. Good agreements between DEM, Finite Element and theoretical results prove the capability of this developed DEM approach for modelling the elastic behaviour of general FRP composite lamina and laminates.

Key words: FRP, composite laminates, DEM, Anisotropic materials, Elasticity behaviour

1. Introduction

Glass fibre and carbon fibre reinforced polymer composite laminates, i.e. GFRP and CFRP, have been widely used in aerospace, mechanical and civil engineering mainly due to their high stiffness-weight ratios. In addition, with proper design and optimization of the layer-up, desired modulus and strength in different directions of the laminates can be

*Corresponding author
Email addresses: D.Yang@leeds.ac.uk (Dongmin Yang)

achieved. However, due to the complexity of the microstructure of FRP composite laminates, the onset of damage does not cause instantaneous failure of the entire structure.There exists a progressive process from the damage initiation to final structural collapse [1]. Thus it is much more challenging to predict the strength of a FRP composite laminate than that of conventional homogenous materials and structures. Understanding of the failure mechanisms as well as developing accurate and universal failure criteria for predicting the ultimate strength of FRP composite laminates, particularly under triaxial loads, is therefore of significant importance. There are a number of failure criteria being developed and some of them have been implemented in finite element software packages. For instance, Hashin failure criteria [2] in ABAQUS and Tsai-Wu failure criterion [3] in ANSYS. Recent exercises, the Second World Wide Failure Exercise (WWFE-II), of assessing some existing failure criteria for FRP composite laminates have shown satisfactory performance of each criterion to various degrees, however, it was concluded from WWFE-II that '*no one model contains all what is required to produce a robust and reliable tool for designers*' [4]. There are also considerable variations in the accuracy of the predictions by these criteria. One of the main reasons for this is that some of those failure criteria are not capable of dealing with the damage progression after the occurrence of first failure. It is recognised from the exercises that failure criteria capable of distinguishing various failure modes and their interactions would be more potent to be adopted by the industry. This poses a big challenge on experimental tests to obtain valid results for calibrating the predictions of damage progression from the failure criteria. While it is already mentioned in the WWFE-II exercise that lacking of test data, particularly under high hydrostatic pressure, has resulted in incomplete failure envelope for benchmarking the failure criteria. The monitoring and visualization of in-situ damage progression during mechanical tests is no doubt very difficult and produce valid data. More recently, the third World-Wide Failure Exercise (WWFE-III) was conducted to highlight the degree of maturity of twelve internationally recognised approaches (some of them are different from the criteria mentioned in WWFE-II) considering their capabilities of detecting the various damages within the composite materials when subjected to multi-axial loading [5, 6, 7]. Thirteen cases were adopted to test the cracking and failure propagation

arising from ply thickness, lay-up sequence, size effects and various loading conditions of unidirectional and multi-directional GFRP and CFRP composite laminates. It was found that any two models cannot give identical predictions for any of the 13 test cases. In few cases, the ratio between the highest and lowest predictions can reach a factor of 20. Still, progressive cracking or damage cannot be predicted by any of the model for a lamina under the shear and transverse loading [7]. Meanwhile, there was still a lack of agreement between these tested models when it comes to the effects of ply thickness, lay-up sequence, and delamination driven by the matrix cracking, etc. Recently, a big step forward improve the understanding of the crack initiation in FRP composite laminates has been made by using synchrotron-radiation computed tomography (SRCT) and acquiring high-resolution, in-situ images of cracks for more accurate measurement of the location, shape and size of small cracks in the order of 1 micrometre [8, 9]. This promising in-situ testing technology can provide more quantitative validations of numerical models in terms of damage progression from one type of failure to another.

For a long time, numerical modelling of damage progression in FRP composite laminates has been reported using Finite Element Method (FEM) [10, 11, 12, 13, 14], Boundary Element Method (BEM) [15, 16, 17, 18] as well as Discrete Element Method (DEM) [19, 20, 21, 22]. The FEM and BEM methods are based on continuum mechanics and are capable of accurately predicting stress distribution as well as crack initiation, but the crack propagation and intersection is always challenging to deal with by these methods. The DEM is based on discontinuous mechanics and uses discrete particles that are bonded together to represent the continuity of FRP composite materials. As the particles only interact with the neighbouring particles through contacts and bonds, fracture events are accounted for at the local level by the breakage of bonds. This gives an advantage to DEM when modelling the damage progression. However, DEM employs explicit time integration scheme to track the motion of individual particles and their interaction, thus it is relatively more expensive in terms of computational efficiency, in particular when the detailed material microstructures are considered. In addition, when particles are randomly packed, it is not straightforward, if possible, to determine the microscale bond and particle properties in order to represent

the elasticity and failure strength of the target material. Trial and error tests are usually required to calibrate the bond and particle properties through virtual mechanical tests, e.g. compressive test and Brazilian test, etc. Also large number of particles are required for any random packing model to represent for the anisotropy of the composite. Therefore, to improve the computation efficiency in some cases, the particles are packed in a regular form, e.g. hexagonal or square in 2D and face-centred cubic or hexagonal in 3D. In principal a theoretical formula can be derived to correlate the particle and bond stiffness (i.e. micro stiffness) with real material elastic stiffness (i.e. macro stiffness). Based on average strain energy method, formulations for both isotropic and anisotropic materials in 2D and isotropic materials in 3D have been derived and employed in various studies [23, 24, 25, 26]. In the previous works by the authors, based on the theoretic formula for bonded particles in a hexagonal packing, 2D DEM model of cross-ply composite laminates have been developed to investigate the damage progression of transverse cracking and delamination [1, 21]. However, in practice many FRP composite laminates are angle-ply laminates in which not all layers are placed either in 0 or 90 degrees. Therefore a 3D DEM model should be developed to model the damage progression in angle-ply FRP composite laminates, and a rigorous formula for describing the relationship between micro and macro stiffness is required. For a DEM model of a composite with single or a few carbon fibres which are orthotropic, a formula is also required to determine the bond stiffness of particles. In view of these constraints on 3D DEM models and to enhance the capability of DEM in modelling damage progression, a theoretical relationship between the bond stiffness in 3D DEM models and the real material stiffness is required.

The present study aims to develop 3D DEM modelling approaches to represent the anisotropic elasticity of the composite materials. Three different approaches have been tested and the most appropriate approach for the general anisotropic composites has been identified and recommended. 3D discrete lattice approach, 3D Hexagonal Close Packing (HCP) approach and extended 2D Hexagonal and Square Packing approach are considered and evaluated. The following sections of this paper are organized as bellow: the background of theory and formulation for DEM and these three approaches are presented in Section 2.

The three DEM models of the 0° ply composite lamina are described in Section 3, in which the comparison and evaluation are made. In Section 4, typical angle-ply laminae and two composite laminates were built with the chosen model and validated against the theoretical and FEM results. Finally, conclusions and recommendations are made in Section 5.

2. 3D DEM theory and microplane theory

2.1. 3D DEM theory

In the DEM, the interaction between the contacting particles is treated as a dynamic process and the stress and deformation of the whole particles assembly are obtained from the average of the force and displacement of each individual particle. The contact which connects the two particles can be physically represented through springs, friction resistance and damp absorber, as shown in Figure. 1 [27].

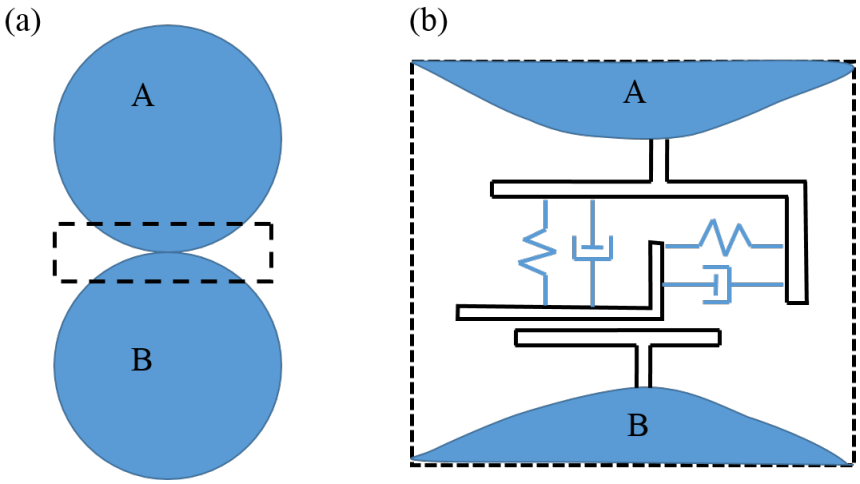

Figure 1: Representation of a contact between two particle elements in 3D DEM: (a) two particles in contact and (b) the physical elements of the contact

The dynamic behaviours of particles in DEM is completed through the integration of particles accelerations and velocities by using a central-difference scheme with an explicit time-step algorithm. The calculation of DEM is alternatively performed by Newtons second law and force-displacement law. Newtons second law is used to calculate the particles acceleration resulting from the contact forces and external forces, while the force-displacement

law is used to update the contact forces according to the relative displacement of the two contacting particles. These two laws are applied repeatedly to form the whole calculation cycle of DEM, as shown in Figure 2.

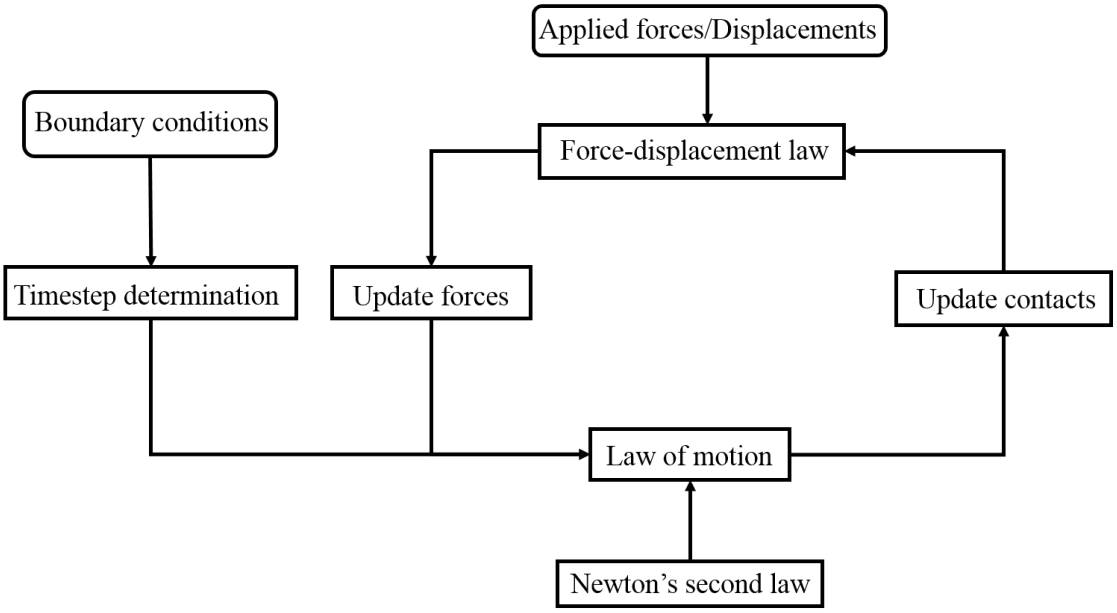

Figure 2: Calculation cycle of DEM

Therefore, DEM is particularly suitable to dynamically simulate the particle systems, in which the movement of every particle is essential to monitor and analyse. The discrete particles can also be densely packed and bonded together by adding special bonds at the contact points corresponding to special constitutive equations.

2.2. Bonded particle model in 3D DEM

Particles in DEM can be bonded together at contacts and separated when the bond strength or energy is exceeded. Therefore it can simulate the motion of individual particles and also the behaviour of bulk material which is formed by assembling many particles through bonds at contacts.

The advantage of this method is that the two bonded particles can be separated and thus a crack is formed at the contact point once the failure condition of the bond is satisfied. In a DEM model, elementary micro scale particles are assembled to form the bulk material

with macroscopic continuum behaviour determined only by the dynamic interaction of all particles. Unlike the conventional FEM that is based on the traditional continuum mechanics and provides stress and displacement solutions by solving a global stiffness matrix equation, DEM is discontinuous and the information of each particle element and contact is recorded individually and updated dynamically. Thus, DEM is convenient to deal with local behaviour of a material by defining local models or parameters for the specified particles and contacts. Subject to external loading, when the strength or the fracture energy of a bond between particles is exceeded, flow and disaggregation of the particle assembly occur and the bond starts breaking [27]. Consequently, cracks form naturally at micro scale. Hence, damages and their interaction emanate as the process of debonding of particles. The way that DEM discreties the material domain gives the most significant advantage over the traditional continuum methodologies, such that problems like the dynamic material behaviour of composites, crack tip singularities, crack formulation criterions can all be avoided due to the naturally discontinuous representation for material microstructure via particle assemblies. Therefore, DEM has been applied in the simulation of crack or damage in rock [28], concrete [29], ceramic [30] and composite materials [1].

DEM and lattice method are both discrete approaches. In DEM, the positions of particles can evolve, so that neighbours of particles might change during analysis. Therefore, DEM models are suitable to describe processes involving large displacements or dynamic behaviour. On the other hand, in lattice models the connectivity between nodes at regular positions is treated as elastic beam which are not changed during the analysis, so that contact determination is not required and the computation efficiency is higher. Consequently, lattice models are mainly suitable for analysis involving small strains [31]. In lattice model, when a facture takes place, the corresponding beam is removed and element-element post-failure friction normally is not taken into account, which does not reflect real mechanical behaviour particularly when the material is under compressive loading. Actually in DEM, when a regular assembly of particles is used, the model is quite similar to lattice models [32]. Bonds in DEM can be envisioned as a kind of glue joining the two contacting particles. In this paper we use the parallel bond which can be regarded as a set of elastic springs with

constant normal and shear stiffness, uniformly distributed over either a circular or rectangular cross-section lying on the contact plane and centred at the contact point, as shown in Figure 3 [27]. Parallel bond can transmit both force and moment.

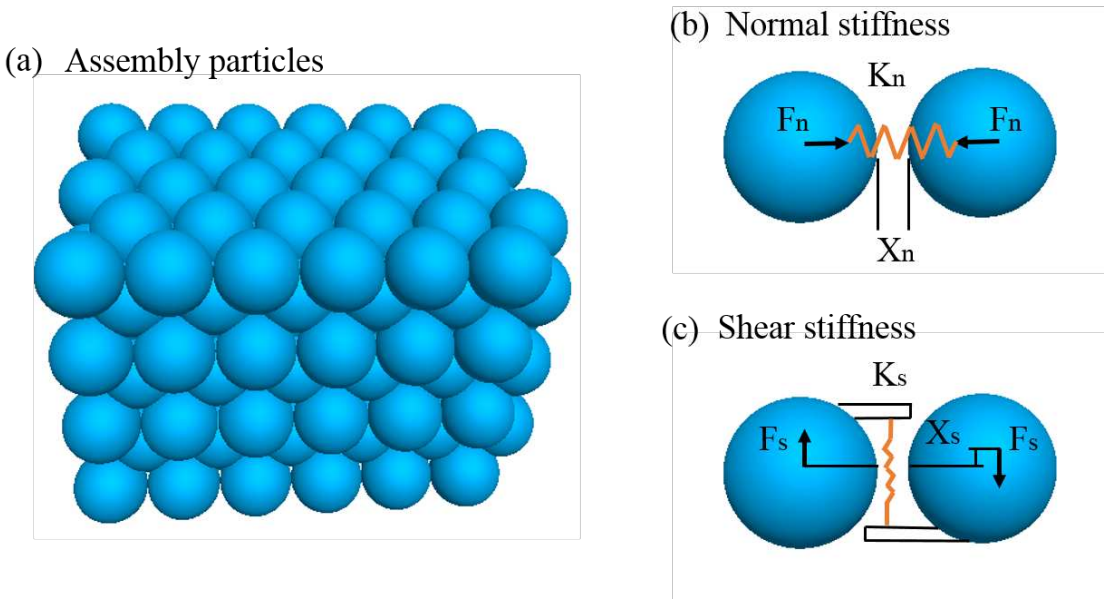

Figure 3: Parallel bond in DEM

In the DEM model with parallel bonds, the contact stiffness, K_i, at each particle-particle contact is resulted from both particles' stiffness and parallel bond's stiffness through the following formulations [27],

$$K_i = A\bar{k}_i + k_i \tag{1}$$

$$A = 2\bar{R}\delta \tag{2}$$

$$K_i = \frac{k_i^{[A]} k_i^{[B]}}{k_i^{[A]} + k_i^{[B]}} \tag{3}$$

where $\bar{R}$ and A are the radius and cross-section area of the parallel bond, respectively. δ is the element thickness, $\bar{k}_i$ is the parallel bond stiffness and k_i is the equivalent stiffness of the two contacting particles. i is in place of n or s, which indicates normal or shear direction, respectively.

The elasticity of a particle assembly with bonds is determined by the constant stiffness when particles are regularly packed, each particle has a defined number of contacts with

other particles at specific contact position on the particle surface and it is possible to have a theoretical relationship between the model's elasticity and particle-particle contact/bond stiffness, even when the moduli elasticity is anisotropic. To achieve this, microplane theory has to be adopted, which is classified in the next section.

When a bonded particle model is used in DEM to represent solid materials, one first needs to determine the bond and particle stiffness in the model ('micro-stiffness') so as to represent the elasticity ('macro-stiffness') of the real target material. In principle it is possible to establish a theoretical relationship between the micro and macro stiffness when particles are packed in a regular form and unit cell can be identified. Formulation for square or hexagonal bonded particles in 2D DEM models of both isotropic and orthotropic materials have been reported in previous literature either using average strain energy method [33] or discrete element method [34, 35]. The regular packing of 3D particles is much more complex, even just for a DEM model of isotropic material. Zhao et al. [36] applied the internal bond method and average strain energy method to correlate the bond stiffness with the real material elastic stiffness. Liu et al. [37] derived a conversion formulas to correlate inter-element parameter with rock mechanical properties with 3D discrete element method. Microplane theory was employed to identify the beam stiffness in a 3D lattice model of transversely isotropic rock material, in which the particles are randomly packed and are allowed to interact with their neighbours that are not necessary in contact as shown in Section 3.1. However, to the author's best knowledge, there is no such a formulation for 3D DEM models of anisotropic or transversely isotropic materials reported in the literature.

2.3. Microplane theory

The microplane model assumes the macro stress and strain tensors are resolved into stress and strain vectors on various microplanes with different orientation in the material, and the stress-strain relationship is independent on those microplanes [38]. The microplane model can be seen in Figure 4, in which the stress can be calculated by the strain.

Variational principle is then used to relate the stress and strain vector on the microplanes to the macroscopic stress and stain tensors. Because the constitutive law is formulated on

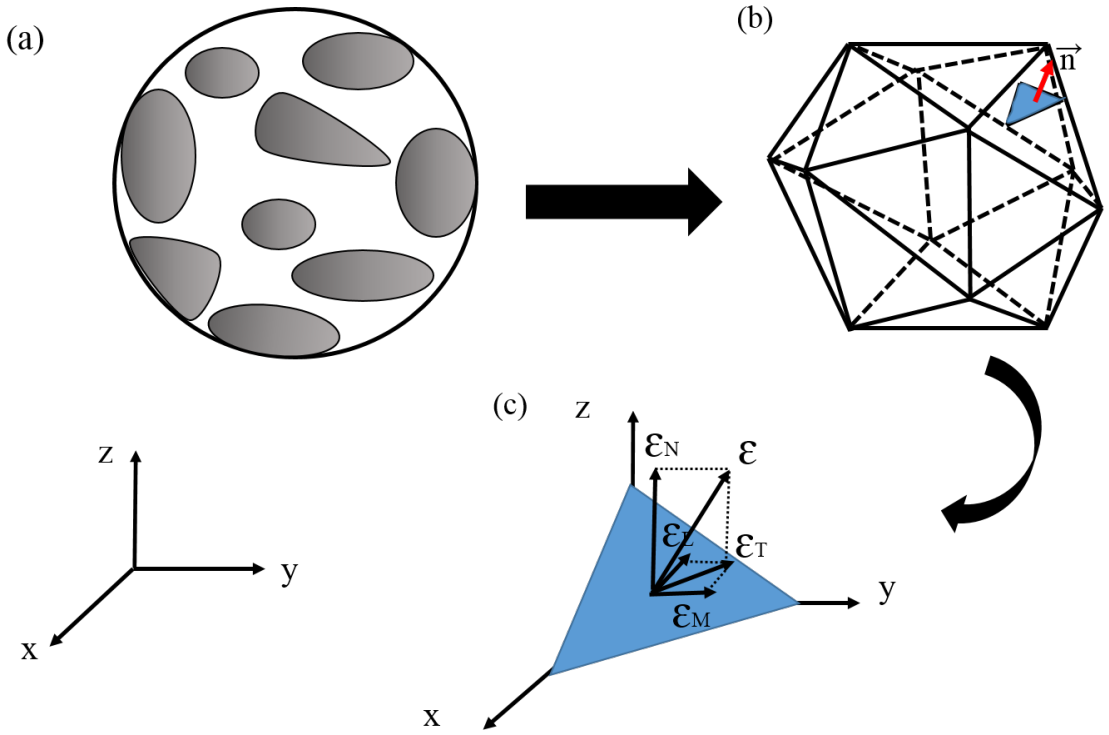

Figure 4: (a) system of discrete microplanes; (b) Microplane strain vector and its components; (c) microplane strain components [39]

discrete microplanes, the fracture of material is naturally accounted for by spatial distribution of cracks on the specified microplanes. Since 1980s, microplane model has been successfully applied to predict the facture behaviour of rock [40], concrete [41], composite sandwich plates [42] and FRP composite laminates [43].

From a numerical discretisation point of view, the continuum-based microplane model discretises a continuous domain into various microplanes ('break down') whilst discontinuum-based discrete element method use artificial bonds to assemble discrete particles together to represent a continuum ('build up'). Although these two methods are originated from different subjects and are theoretically different, they actually predict almost the same elastic behaviour of materials with a particular microstructure [44]. This also suggests that if a DEM model and a microplane model are constructed in a way such that the bond positions are identical to the microplane orientations, then it is expected that the bond

stiffness (if particle stiffness is ignored) is the same as the microplane stiffness, and they can both be referred as 'contact stiffness'.

The microplane model used in this study is provided by Carol et al. [45], where the normal and shear moduli are E_N and E_T, respectively. Considering the unit hemisphere denoted as Ω, the elastic stiffness tensor C is shown as below:

$$C = \frac{3}{2\pi} \int_{\Omega} (E_N N \otimes N + E_T T^T \cdot T) \, \mathrm{d}\Omega \tag{4}$$

Assuming that the particles are regularly packed and the strain is uniformly distributed in the particle assemble and then using virtual work principle the relation of the contact stiffness to the material elasticity tensor is derived as [44, 46]:

$$C = \frac{1}{V} \sum \|l\|^2 [k_N N \otimes N + k_T T^T \cdot T] \tag{5}$$

where V is the average volume of the unit cell that one particle occupies in space, l is the distance between the centroids of two contacting particles, k_N and k_T are the normal and tangential stiffness, respectively, and N and T are the normal and tangential projection tensors on the contact plane, respectively, which are further interpreted as below [44]:

$$N \otimes N = n_i n_j \otimes n_k n_l = n_i n_j n_k n_l \tag{6}$$

$$T = n \cdot I^{sym} - n \otimes n \otimes n = \frac{1}{2} n_l (\delta_{lj}\delta_{ik} + \delta_{lk}\delta_{ij}) - n_i n_j n_k \tag{7}$$

$$T^T = I^{sym} \cdot n - n \otimes n \otimes n = \frac{1}{2} n_l (\delta_{ik}\delta_{jl} + \delta_{il}\delta_{jk}) - n_i \tag{8}$$

$$T^T \cdot T = \frac{1}{4} n_j n_k \delta_{il} + \frac{1}{4} n_j n_l \delta_{ik} + \frac{1}{4} n_i n_k \delta_{jl} + \frac{1}{4} n_i n_l \delta_{jk} - n_i n_j n_k n_l \tag{9}$$

where I^{sym} is the fourth-order symmetric unit tensor , n is the unit normal vector of the contact plane and δ is the Kronecker delta. The orientation of microplane could be random or regular in space. In DEM, these microplanes of a particle are the contact planes or between the particle and its neighbours.

3. 3D DEM modelling of composite laminae

In 3D DEM modelling of composite lamina, three different models are considered in this study: 3D discrete lattice model, 3D Hexagonal Close Packing (HCP) model and Ex-

tended 2D Hexagonal and Square models. 3D discrete lattice model introduces a model based on the modified DEM formulation originally aiming at modelling the rock behaviour with transversely isotropic elasticity [47]. 3D Hexagonal Close Packing (HCP) model is a model based on the 3D DEM theory with a representative packing way aiming at modelling the anisotropic property of the composite lamina. And the Extended 2D Hexagonal and Square models are the models with the assumption of plane stress aiming at modelling the anisotropic material such as composite lamina. All of these three models are discussed in this section. The different colour balls (such as blue and red) at both sides in all the models represent the boundary where the velocity is applied. The bonds between the two group of balls represent the different stiffness of fibre and matrix, where the balls for creating the bonds are hidden.

Considering the material in these simulations, a test example (E-Glass/MY750) is adopted from WWFE-II [48]. The material properties are listed in Table 1.

Table 1: The material mechanical property of composite lamina with E-Glass/MY750 [48]

	E_1 (GPa)	E_2= E_3 (GPa)	G_{12}	υ_{12}=υ_{21}	υ_{23}
E-Glass/MY750	45.6	16.2	5.83	0.278	0.4

3.1. 3D discrete lattice model in DEM

As mentioned above, this approach is originally aiming at modelling the transversely-isotropic elasticity of the rock behaviour with the modified DEM theory [47]. However, here this approach will be applied to model the transversely-isotropic elasticity of composite lamina. This approach is based on the microplane theory and assumptions such as the Voigt hypothesis, geometrically isotropic lattice and two element orientation dependent stiffnesses.

In this approach, the Voigt hypothesis can be achieved by enlarging the contact distance between the particles, even not geometrically neighbouring. In DEM, the lattice satisfying the Voigt hypothesis can be constructed by a group of particles in which all of the contacts between particles should follow the assumption below:

$$|x_1 - x_2| \leq I_R(r_1 + r_2) \tag{10}$$

where x_i and r_i are the position and radius of the sphere particle, respectively. I_R is the contact radius and a dimensionless parameter which can determine the lattice's density. If the I_R equals to 1, that means only geometrically neighbouring particles are considered to be in contact, while greater values allow the two particles to be 'contact' even in some distance between them. The 3D periodic lattice illustrated in Figure 5 has a contact radius of 1.8 which is proved to be realistic in Ref. [47].

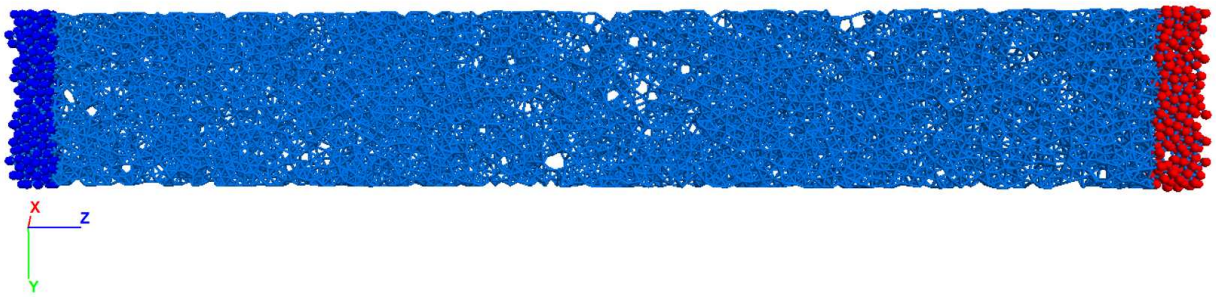

Figure 5: 3D discrete lattice model with a contact radius of 1.8

In this case, z-axial is coincident with the transversely-isotropic axial, θ and φ are the inclination angle from the pole and the azimuth angle in spherical coordinates, respectively. The stiffness tensor is calculated by the integration of moduli over all possible orientations of microplanes decided by the unit vector n, which is based on the equation (4). Here, $E_N = E_N(\theta)$ and $E_T = E_T(\theta)$, which are independent of the φ.

$$C = \frac{3}{2\pi}\int_{\theta=0}^{\pi}\int_{\varphi=0}^{2\pi}(E_N N \otimes N + E_T T^T \cdot T)\sin\theta \,\mathrm{d}\varphi \,\mathrm{d}\theta \tag{11}$$

Combining with equations (6), (7), (8), 9, we can obtain the stiffness tensor components as below:

$$\begin{aligned} C_{ijkl} = \frac{3}{2\pi}\int_{\theta=0}^{\pi}\int_{\varphi=0}^{2\pi}(E_N(\theta)(n_i n_j n_k n_l) + E_T(\theta)(\frac{1}{4}n_j n_k \delta_{il} + \frac{1}{4}n_j n_l \delta_{ik} \\ + \frac{1}{4}n_i n_k \delta_{jl} + \frac{1}{4}n_i n_l \delta_{jk}) - n_i n_j n_k n_l)\sin\theta \,\mathrm{d}\theta \,\mathrm{d}\varphi \end{aligned} \tag{12}$$

In this case, the moduli $E_N(\theta)$ and $E_T(\theta)$ can be assumed as a function interpolating with moduli E_N^a and E_N^b in terms of θ, such as

$$E_N(\theta) = sin^2(\theta)E_N^a + cos^2(\theta)E_N^b \tag{13}$$

In the same way, the $E_T(\theta)$ can be written as

$$E_T(\theta) = cos^2(\theta)E_T^a + sin^2(\theta)E_T^b \tag{14}$$

Here the θ is continuous in (0, $\pi/2$) and symmetrical around $\pi/2$ as well. The elliptic interpolation of the stiffness can be shown below in Figure 6:

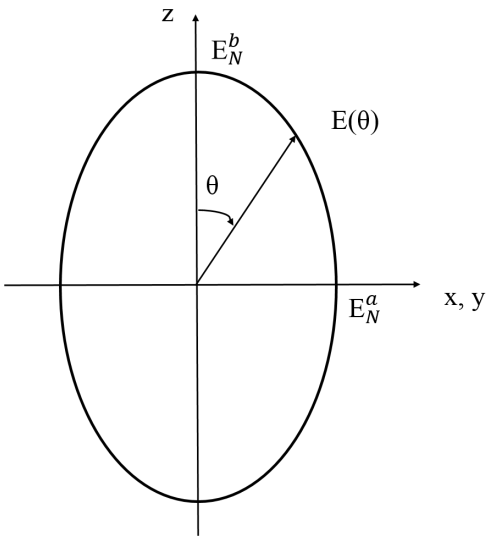

Figure 6: Elliptic interpolation of stiffness [47]

Then all the stiffness tensor components as a function of lattice moduli can be obtained as below:

$$\begin{pmatrix} C_{1111} \\ C_{3333} \\ C_{2233} \\ C_{1122} \end{pmatrix} = \begin{pmatrix} C_{11} \\ C_{33} \\ C_{13} \\ C_{12} \end{pmatrix} = \frac{1}{35} \begin{pmatrix} 36 & 6 & 20 & 8 \\ 12 & 30 & 16 & 12 \\ 8 & 6 & -8 & -6 \\ 12 & 2 & -12 & -2 \end{pmatrix} \begin{pmatrix} E_N^a \\ E_N^b \\ E_T^a \\ E_T^b \end{pmatrix} \tag{15}$$

Based on the traditional composite laminate theory, the stiffness tensor can be solved and then the E_N and E_T will be resolved from the equation (15) to build the 3D lattice discrete model which will be discussed in Section 3.4.

3.2. 3D HCP model in DEM

As an attempt to build a 3D DEM model for anisotropic composite material, particles are packed in a regular form so that the particle position and contact are fixed for later

calculations. In addition to the microplane model, internal bond model, average stress method were also used for 3D isotropic DEM models, here the microplane model is adopted with a purpose of comparison with the 3D lattice discrete model of transversely isotropic materials which is based on microplane model.

In this approach, the particles are packed in a hexagonal form, and in the centre plane, the stiffness of particle 0 could affect the contact stiffness between particle 0 and the six surrounding particles. On the other hand, the parallel bond can be applied at each contact and its stiffness can be chosen at various values. Therefore the parallel bond stiffness $\bar{k}_i$ is expected to contribute the most to the contact stiffness K_i, and the particles' stiffness k_i is set to be much smaller than the one of parallel bond in order to achieve the required contact stiffness at different contacts accordingly [27], e.g.

$$k_i = 0.01A\bar{k}_i \tag{16}$$

and

$$K_i \approx A\bar{k}_i \tag{17}$$

To better achieve a uniform strain distribution, closer packing of particles is preferred. There are two close packing styles for particles in 3D, Cubic Close Packing (CCP) and Hexagonal Close Packing (HCP) [49]. In this study, the Hexagonal Close Packing is mainly adopted for the 3D modelling. Consider a representative particle, white particle in layer B in Figure 7, it has six contacting neighbours in the same layer, three contacting neighbours in both upper layer C and lower layer A, i.e. 12 contacts and 24 contact stiffnesses in total, and the detail is shown in Figure 8. The position and orientation of each contact plane is known thus k_N and k_T are known for each contact. By using symmetry the number of the unknown contact stiffness in E could be reduced to exactly match the number of constants in the stiffness tensor C, so that a unique solution of micro contact stiffness can be obtained.

The unit normal vector of the contact plane between two particles n is written in spherical

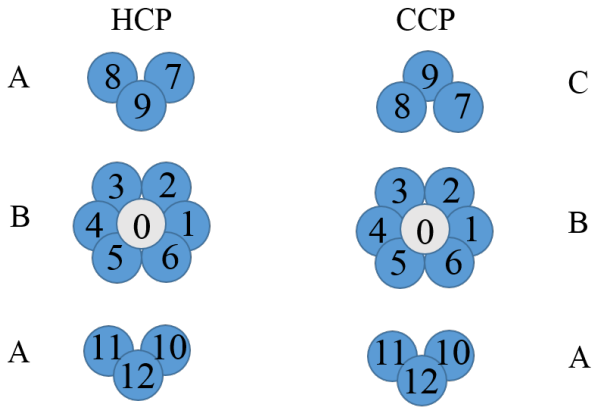

Figure 7: (a) HCP packing and (b) CCP packing [50]

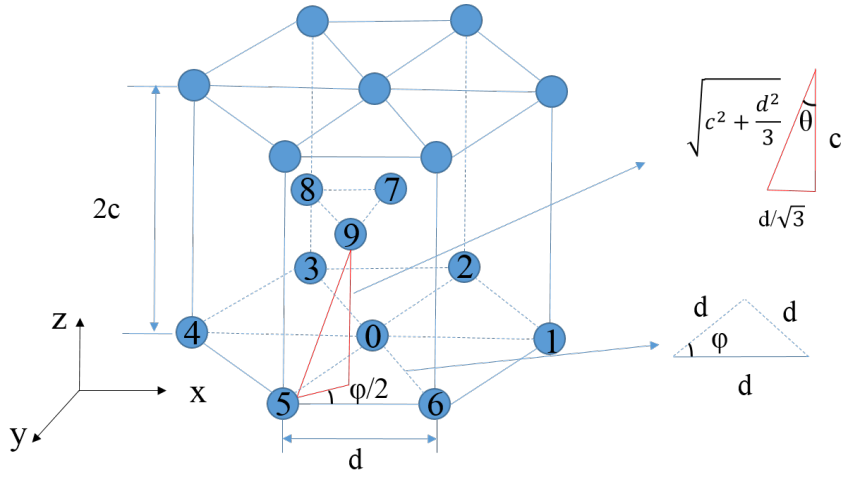

Figure 8: 3D HCP packing of DEM particles

coordinate system as

$$n = \begin{pmatrix} x \\ y \\ z \end{pmatrix} = \begin{pmatrix} sin\theta cos\varphi \\ sin\theta sin\varphi \\ cos\theta \end{pmatrix} \tag{18}$$

where d is the distance between the two particles centre, θ is the angle between the straight line of ball nine in the A layer and ball five in the B layer and the vertical line, φ is the angle of different adjacent balls in the unit triangle. Setting the centre of particle 0 as the origin of the coordinate system and assuming the fibre direction is aligned with X axis, one

can easily determine the unit normal vector of each contact plane of particle 0.

The volume of a sphere particle is

$$V_{sphere} = \frac{4}{3}\pi R^3 \tag{19}$$

And the average density (packing efficiency) of HCP and CCP is

$$\rho_{HCP} = \rho_{CCP} = \frac{4 \times \frac{4}{3}\pi R^3}{16\sqrt{2}R^3} = \frac{\pi}{3\sqrt{2}} \tag{20}$$

Thus the average volume occupied by a sphere in HCP and CCP is

$$V_{unitcell} = \frac{V_{sphere}}{\rho_{HCP}} = \frac{V_{sphere}}{\rho_{CCP}} = \frac{\frac{4}{3}\pi R^3}{\frac{\pi}{3\sqrt{2}}} = 4\sqrt{2}R^3 \tag{21}$$

Thus the stiffness tensor C in equation (5) can be written as:

$$C_{ijkl} = \frac{1}{4\sqrt{2}R^3}(2R)^2 \sum_{c=1}^{12}[k_N^c(n_i n_j n_k n_l) + k_T^c(\frac{1}{4}n_j n_k \delta_{il} + \frac{1}{4}n_j n_l \delta_{ik} + \frac{1}{4}n_i n_k \delta_{jl} + \frac{1}{4}n_i n_l \delta_{jk}) - n_i n_j n_k n_l] \tag{22}$$

where R is the radius of the particle. In the DEM model can be developed according the macro material stiffness tensor. Considering a single transversely isotropic FRP lamina which has 5 engineering constants, i.e. E1, E2=E3, G12=G13, v12=v13, v23, its fibre direction is aligned with X axis, then there are 5 corresponding independent constants in the stiffness matrix, C_{11}, C_{12}, C_{22}, C_{23}, C_{66}, which can be represented by the engineering constants as below: (i.e., C_{66}=C_{1212}=C_{1313})

$$[C] = \begin{bmatrix} \frac{1-\nu_{23}}{\delta}E_1 & \frac{\nu_{12}}{\delta}E_2 & \frac{\nu_{12}}{\delta}E_2 & 0 & 0 & 0 \\ & \frac{1-\nu_{12}^2\frac{E_2}{E_1}}{(1+\nu_{23})\delta}E_2 & \frac{\nu_{23}+\nu_{12}^2\frac{E_2}{E_1}}{(1+\nu_{23})\delta}E_2 & 0 & 0 & 0 \\ & & \frac{1-\nu_{12}^2\frac{E_2}{E_1}}{(1+\nu_{23})\delta}E_2 & 0 & 0 & 0 \\ & & & \frac{E_2}{2(1+\nu_{23})} & 0 & 0 \\ & \text{sym.} & & & G_{12} & 0 \\ & & & & & G_{12} \end{bmatrix} \tag{23}$$

with the parameter $\delta = 1 - \nu_{23} - 2\nu_{12}^2\frac{E_2}{E_1}$. We have the condition $\delta > 0$.

By symmetry, in the layer A, B, C it is assumed that

$$\begin{cases} k_n^1 = k_n^4 \\ k_n^2 = k_n^3 = k_n^5 = k_n^6 = k_n^7 = k_n^8 = k_n^9 = k_n^{10} = k_n^{11} = k_n^{12} \\ k_t^1 = k_t^4 \\ k_t^2 = k_t^3 = k_t^5 = k_t^6 = k_t^7 = k_t^8 = k_t^9 = k_t^{10} = k_t^{11} = k_t^{12} \end{cases} \tag{24}$$

In this approach, the distance c between layer A and layer B is introduced, so there are five variables (i.e. C_{11}, C_{12}, C_{22}, C_{23}, C_{66}) needed for transversely isotropic material which is corresponding to 4 stiffness constants (i.e. k_n^1, k_t^1, k_n^2 and k_t^2) and the distance c. In Figure 8, it can be found that

$$sin\theta = \frac{2r}{\sqrt{3c^2 + 4r^2}}, cos\theta = \frac{\sqrt{3}c}{\sqrt{3c^2 + 4r^2}} \tag{25}$$

Using the equation (22) and the stiffness relations between different balls, the following relationship between C_{ijkl} and $k_{n,t}$ can be obtained

$$\begin{cases} C_{1111} = \frac{1}{\sqrt{2}R}[2k_N^1 + (\frac{1}{4} + \frac{9}{4}sin^4\theta)k_N^2 + k_T^2(\frac{3}{4} + 3sin^2\theta - \frac{9}{4}sin^4\theta)] \\ C_{1122} = \frac{1}{\sqrt{2}R}[(\frac{3}{4} + \frac{3}{4}sin^4\theta)k_N^2 - k_T^2(\frac{3}{4} + \frac{3}{4}sin^4\theta)] \\ C_{2222} = \frac{1}{\sqrt{2}R}[(\frac{9}{4} + \frac{9}{4}sin^4\theta)k_N^2 + k_T^2(\frac{3}{4} + 3sin^2\theta - \frac{9}{4}sin^4\theta)] \\ C_{2233} = \frac{1}{\sqrt{2}R}[3sin^2\theta cos^2\theta k_N^2 - 3sin^2\theta cos^2\theta k_T^2] \\ C_{1212} = \frac{1}{\sqrt{2}R}[(\frac{1}{2}k_T^1 + (\frac{3}{4} + \frac{3}{4}sin^4\theta)k_N^2 + k_T^2(\frac{3}{4} + \frac{3}{2}sin^2\theta - \frac{3}{4}sin^4\theta)] \end{cases} \tag{26}$$

3.3. Extended 2D hexagonal and square models in DEM

In this approach, the lamina is a unidirectionally reinforced and is assumed to be in a plane stress state by defining $\sigma_3 = 0$, $\tau_{23} = 0$, τ_{31}=0. We should note that three dimensional stress-strain relationship, the plane stress state on a lamina is not merely an idealization of reality, but it is still a practical and achievable way to analyse the performance of fibres reacting on the matrix. In this case, the relation between the spring constants and elastic constants was established with the average strain energy method instead of the microplane

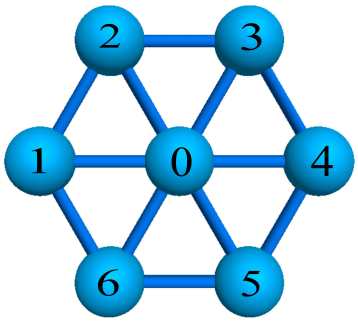

Figure 9: One layer of the 3D DEM model of HCP packing based on 2D packing

theory. In this study, 3D DEM model of the composite lamina was modelled with a six-spring hexagonal packing as a basic unit, as shown below in Figure 9. Each contact between the different particles is modelled with a linear parallel bond which is represented by a set of elastic springs with constant normal stiffness k_n and shear stiffness k_s, respectively. Therefore, these constants of the springs can be related to the macro-scale elastic properties of the material such as Young's Modulus and Poisson's ratio. In this approach, a general formula was adopted from the Liu and Liu [51] with average strain energy method for anisotropic materials, as follows:

$$\begin{cases} k_{n1} = \frac{\sqrt{3}}{6}(3C_{11} + 2C_{12} - C_{22})\delta \\ k_{n2} = \frac{\sqrt{3}}{3}(C_{11} + C_{22} + \sqrt{3}C_{16} + \sqrt{3}C_{26})\delta \\ k_{n3} = \frac{\sqrt{3}}{3}(C_{11} + C_{22} - \sqrt{3}C_{16} - \sqrt{3}C_{26})\delta \\ k_{s1} = \frac{2\sqrt{3}}{3}(3C_{66} - C_{22})\delta \\ k_{s2} = \frac{\sqrt{3}}{3}(C_{22} - 3C_{12} + 3\sqrt{3}C_{16} - \sqrt{3}C_{26})\delta \\ k_{s3} = \frac{\sqrt{3}}{3}(C_{22} - 3C_{12} - 3\sqrt{3}C_{16} + \sqrt{3}C_{26})\delta \end{cases} \tag{27}$$

where k_{n1} and k_{s1} are the normal and tangential spring constants between particle 0 and 1, and particle 0 and 4, respectively; k_{n2} and k_{s2} are the normal and tangential spring constants between particle 0 and 3, and particle 0 and 6, respectively; k_{n3} and k_{s3} are the normal and tangential spring constants between particle 0 and 2, and particle 0 and 5, respectively; δ is the element thickness (here it is the diameter in the lamina). $C_{i,j}(i, j = 1, 2, 6)$ are the

elastic coefficients of the material stiffness matrix, which can be shown in Equation (28):

$$C = \begin{pmatrix} C_{11} & C_{11} & C_{16} \\ C_{12} & C_{22} & C_{26} \\ C_{16} & C_{26} & C_{66} \end{pmatrix} \tag{28}$$

and the reduced stiffness matrix of the material can be obtained by the Young's Modulus and Poisson's ratios within the plane stress state when $C_{16} = C_{26} = 0$,

$$\begin{cases} C_{11} = \frac{E_1}{1-\nu_{12}\nu_{21}} \\ C_{22} = \frac{E_2}{1-\nu_{12}\nu_{21}} \\ C_{12} = \frac{\nu_{12}E_2}{1-\nu_{12}\nu_{21}} \\ C_{66} = G_{12} \end{cases} \tag{29}$$

The 0° ply composite lamina model is built up according to the above approach and mechanical property in the Section 3.4 for the comparison with other two models.

3.4. Comparison and evaluation of three approaches in DEM

In the 3D discrete lattice model, the Poisson ratios should be assumed to be 0.1 as when the ratio was bigger, the E_T^a would be negative. The C_{2323} is calculated to be 41454 MPa from the engineering variables Young's modulus and Poisson ratio, and in order to obtain the targeted moduli we choose the C_{2323} to be the dependent component due to the difficulty in measuring it experimentally and then the in-plane and out-plane moduli were calculated from equation (15) to be

$$\begin{pmatrix} E_N^a \\ E_N^b \\ E_T^a \\ E_T^b \end{pmatrix} = \begin{pmatrix} 3443 \\ 45205 \\ 3017 \\ 15545 \end{pmatrix} (MPa) \tag{30}$$

Once the moduli are obtained, they can be utilized to calculate for the theoretical C_{2323}, which is 13210 MPa. This calculated value is nearly one-third of original one from the engineering constants. Meanwhile, from the theory above, the lattice normal stiffness k_n and

tangential stiffness k_s can be expressed by $E_N(\theta)$ and $E_T(\theta)$ as $k_n = E_N(\theta) * 6V/(N * L^2)$ and $k_t = E_T(\theta) * 6V/(N * L^2)$. As the particle is randomly created, so the bonds (lattice) are also distributed randomly, which means the lattice bonds in this model would be different from each other. In this 3D Lattice DEM model, 8, 841 identical balls were generated randomly in a rectangle box and the bonds were generated if the contact radius which refers to Equation (10) is not bigger than 1.8 to ensure the stability of this model, then 39,311 bonds were generated according to this principle to form a geometrical model with a dimension of 10 mm $\times$ 1 mm $\times$ 0.2 mm. The two spring constants were applied to the bonds according to the rule corresponds to the Section 3.1. The test was conducted with uniaxial unconfined tension load, and the velocity is applied at both left and right sides of the model to be 10 mm/s and cycle 200, 000 times and the automatic time-step is $9.02e^{-9}$s. The results were obtained in the Table 2. Figure 10 shows the normal stiffness of the parallel bonds in this model, where different colours of the bond represent different normal stiffnesses.

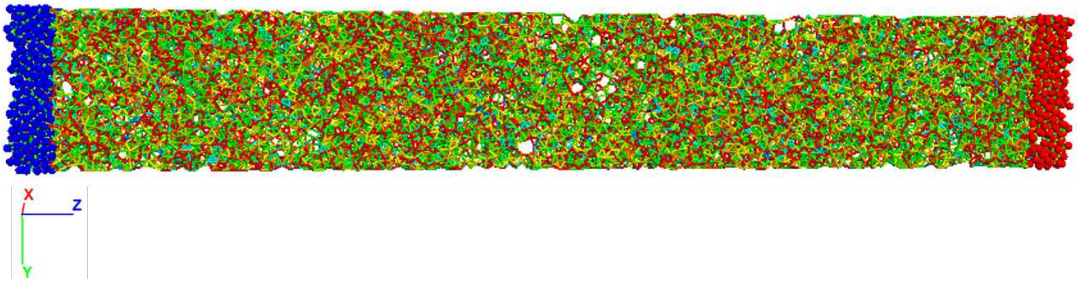

Figure 10: 3D discrete lattice DEM model of 0° ply composite lamina

For the 3D HCP DEM model, the stiffness tensors C_{ijkl} can be calculated with the Classic Composite Laminate Theory and then the k_n and k_s were resolved with the equation (22) as below.

$$\begin{Bmatrix} k_n^1 \\ k_t^1 \\ k_n^2 \\ k_t^2 \end{Bmatrix} = \begin{Bmatrix} 3.6855 \\ 0.0426 \\ 0.8879 \\ 0.0293 \end{Bmatrix} (MPa) \tag{31}$$

These k_n and k_s were applied to the different bonds according to their positions in the

DEM model to calibrate the elasticity of this model. In this 3D DEM HCP model, three layers were adopted to form a single Hexagonal Close Packing for the lamina, and 76×8×3 balls were utilized to generate 8,431 bonds at the adjacent balls. The model dimension is 9.975 mm × 0.93 mm × 0.21 mm. The velocity is applied to the boundary at left and right sides of the model as 10 mm/s, respectively and cycle is 200, 000 times and the automatic time-step is $1.34e^{-8}$s. Figure 11 shows the 3D model of the HCP packing with parallel bonds with different stiffnesses. In this model, the red beams represent the fibre direction with larger k_n, and light blue ones represent the matrix. Meanwhile, when calculating the mechanical property E_2 of this material, x and y coordinate axis should be replaced with each other.

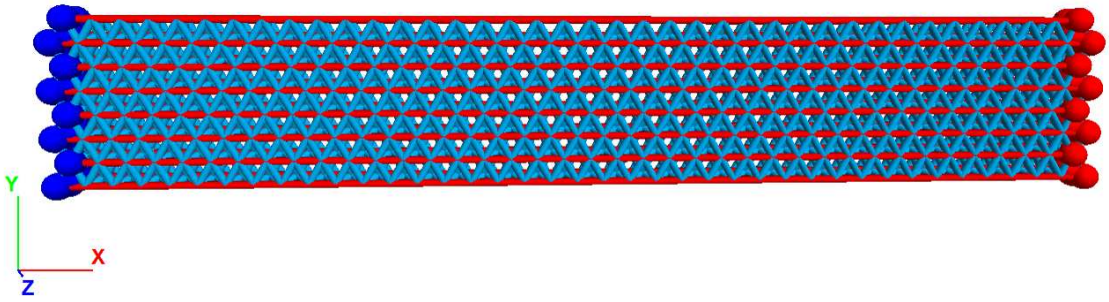

Figure 11: 3D DEM HCP model of 0° ply composite lamina

For the extended 2D hexagonal DEM model, 200×19×2 balls were utilized to create the model for a 0° ply composite lamina with a dimension of 10 mm × 0.83 mm × 0.2 mm. The velocity is applied at both sides as 10 mm/s. In order to ensure numerical convergence of the model, the particles with different radiuses are chosen to build the model, however, it has been found that the radius has no effects on the final results. The balls are used to determine the location of the bonds which are to form the composite lamina/laminates. Meanwhile, the cycle of 200, 000 times is proved to be realistic for this model to obtain a stable simulation results and the automatic time-step is $5.79e^{-8}$s. Figure 12 shows the extended 2D hexagonal DEM model of 0° ply composite lamina, in which the bonds with different colours represent different components in the composite material, such as the red bonds for the fibres and the blue ones for the matrix.

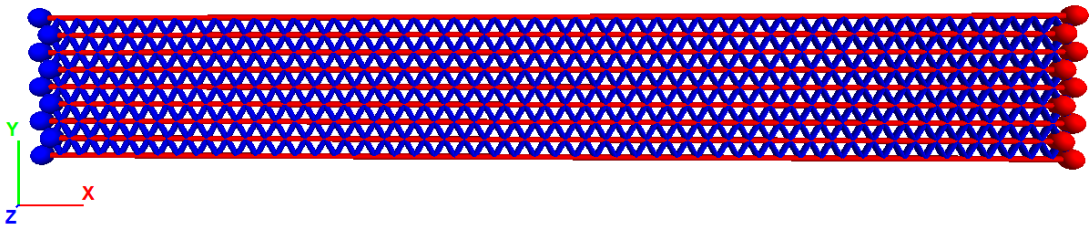

Figure 12: Extended 2D Hexagonal DEM model of 0° ply composite lamina

Table 2 shows the comparison of the simulated results from different approaches against the experimental data for E-Glass/MY750. It can be found that the 3D HCP model and the extended 2D Hexagonal model meet the experimental values well when it comes to the Young's Modulus. However, for the 3D lattice model, it is capable of modelling the lamina of the composite although the Young's Moduli are too small. It can be found that the ratio of experimental Young's Modulus to the simulated one from 3D lattice model is 3.8, moreover, the ratio of C_{2323} calculated from the engineering variables to the C_{2323} calculated from the moduli is 3.14, which is discussed in Section 3.4. More importantly, this approach is very difficult to use when it comes to the bond breaking (i.e. simulation of failure) as one particle can have several bonds with other particles which are not in contact. Meanwhile, the interface between the different layers is also difficult to be determined for laminates, therefore, this approach will not be considered as efficiency for the modelling of laminates. While for the 3D HCP model, reasonable results can be obtained by adjusting the radius of the particles, however, compared to the extended 2D hexagonal model it is more time-consuming as for same dimension and same radius of the particles. The number of particles needed for 3D HCP model is almost three time more than the extended 2D hexagonal model because it has to use three layers for a lamina. Considering the simplicity and efficiency of the model, the extended 2D hexagonal and square model will be constructed in the next section for modelling of the composite laminates.

Table 2: Comparison of three different approaches against experimental results for 0° ply lamina

	E1 (GPa)	E2 (GPa)	υ_{12}	υ_{21}	Computing Time (mins)
Experiments	45.6	16.2	0.278	0.0988	
3D Lattice Discrete model	12.02	4.53	-	0.115	88.5
3D HCP model	47.26	16.0	0.3	0.54	60.5
Extended 2D Hexagonal model	46.03	15.98	0.247	0.104	7.5

4. 3D DEM modelling of composite laminates

In order to model angle-ply composite laminates, a model for angle-ply lamina is also needed to be developed with the extended 2D hexagonal and square modelling approach. For a angle-ply lamina, the reduced stiffness matrix should be transformed from the stiffness matrix (equation 29) for orthotropic materials:

$$\begin{cases} \overline{C}_{11} = C_{11}\cos^4\theta + 2(C_{12}+2C_{66})\sin^2\theta\cos^2\theta + C_{22}\sin^4\theta \\ \overline{C}_{22} = C_{11}\sin^4\theta + 2(C_{12}+2C_{66})\sin^2\theta\cos^2\theta + C_{22}\cos^4\theta \\ \overline{C}_{12} = (C_{11}+C_{22}-4C_{66})\sin^2\theta\cos^2\theta + C_{12}(\sin^4\theta+\cos^4\theta) \\ \overline{C}_{16} = (C_{11}-C_{12}-2C_{66})\sin\theta\cos^3\theta + (C_{12}-C_{22}+2C_{66})\sin^3\theta\cos\theta \\ \overline{C}_{26} = (C_{11}-C_{12}-2C_{66})\sin^3\theta\cos\theta + (C_{12}-C_{22}+2C_{66})\sin\theta\cos^3\theta \\ \overline{C}_{66} = (C_{11}+C_{22}-2C_{12}-2C_{66})\sin^2\theta\cos^2\theta + C_{66}(\sin^4\theta+\cos^4\theta) \end{cases} \tag{32}$$

where $\overline{C}_{ij}(i,j=1,2,6)$ are the elastic constants of the material stiffness matrix for the angle-ply lamina, the θ is the angle of fibres of angle-ply lamina and orthotropic lamina and $C_{ij}(i,j=1,2,6)$ are the elastic constants of the material stiffness matrix for the orthotropic lamina under the plane stress state.

Once the k_n and k_s are obtained from the elastic constants of the composite lamina, the 3D model with the anisotropic properties can be built up. As shown below, different spring constants are applied to the bonds with different orientation in the hexagonal closed packing model in order to obtain the anisotropic property.

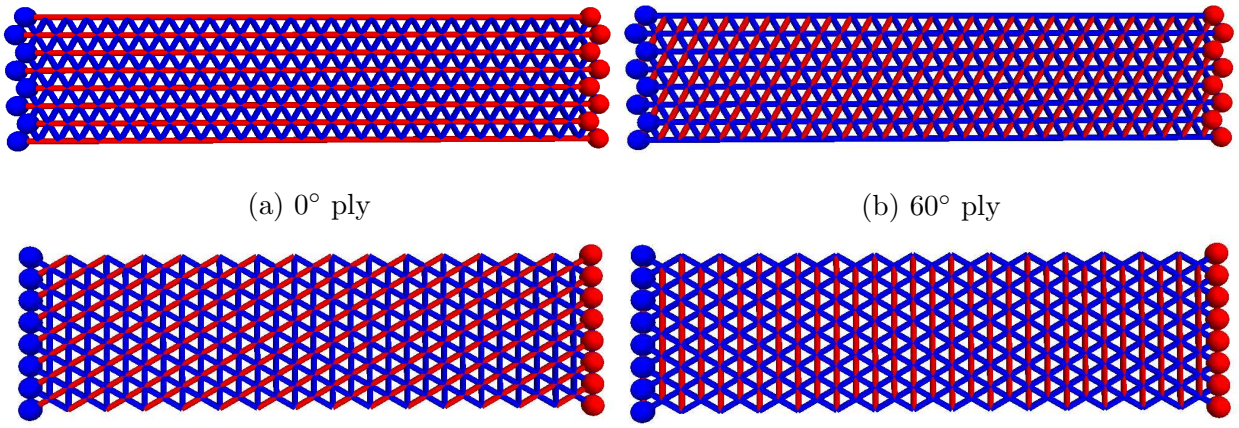

(a) 0° ply (b) 60° ply

(c) 30° ply (d) 90° ply

Figure 13: Extended 2D hexagonal DEM model of angle-ply composite lamina

For comparison, 0° ply lamina and other three different angle plies (30°, 60° and 90°) are modelled, as shown in the Figure 13, the red bonds represent the normal stiffness of fibres and the blue ones represent the normal stiffness of matrix. The load is applied at the blue and red balls on the both sides. The strength of the bonds are set to be very large to prevent them from breaking in order to maintain the elasticity of the model. However, when calculating the 30° and 90° angle-ply lamina, negative k_{s3} occurs which can not be calculated in the PFC software. This is because there is no bond in the direction of 30° and 90° angles in the original model, therefore the x and y axials in the x-y plane, E_1 and E_2, and ν_{12} and ν_{21} are exchanged with each other to obtain the Young's Modulus of above angle-ply laminae. This is the first attempt to model anisotropic property in 3D model. The results are compared in Table 3.

As we can see in the above models, there is no bond located in 45° direction thus we have to choose other packing to achieve this. In this study, we adopted the square packing to model the 45° angle-ply lamina, which is similar to the nine-disc model in the Ref. [51]. However, in their model, only the problem of orthotropic material can be solved, and it is not suitable for the general anisotropic materials. The configuration of the square packing model and the 45° angle-ply lamina are shown in Figure 14.

In this case, regular square lattices are formed with nine balls in which a ball is sur-

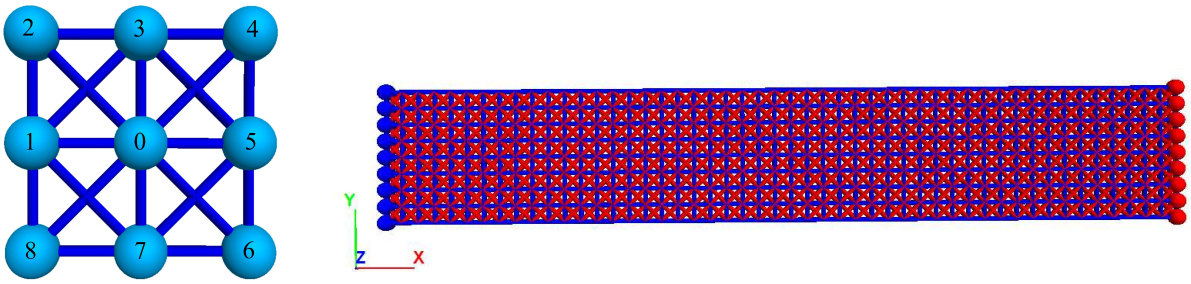

(a) Configuration of square packing

(b) 45° ply composite lamina

Figure 14: Extended 2D square DEM model of 45° angle-ply composite lamina

rounded by other eight balls, shown as Figure 14a. Assuming k_{n1} and k_{s1} are the normal and tangential spring constants between particle 0 and 1, and particle 0 and 5, respectively; k_{n2} and k_{s2} are the normal and tangential spring constants between particle 0 and 2, between particle 0 and 4, between particle 0 and 6 and between particle 0 and 8, respectively; k_{n3} and k_{s3} are the normal and tangential spring constants between particle 0 and 3, and particle 0 and 7, respectively; δ is the element thickness. $C_{i,j}(i,j=1,2,6)$ are the elastic coefficients of the material stiffness matrix, which can be calculated in Equation 29 in the plane stress state. For orthotropic materials, the k_n and k_s is

$$\begin{cases} k_{n11} = \frac{1}{3}(3C_{11} + C_{12} - 4C_{66})\delta \\ k_{n2} = \frac{1}{3}(C_{12} + 2C_{66})\delta \\ k_{n3} = \frac{1}{3}(C_{12} + 3C_{22} - 4C_{66})\delta \\ k_s = \frac{2}{3}(C_{66} - C_{12})\delta \end{cases} \tag{33}$$

It has been reported in [51] that this model is only suitable for orthotropic materials instead of general anisotropic material, however in this study, the 45° virtual fibre direction in the lamina are constructed by transforming the reduced stiffness from the orthotropic material to the general anisotropic material lamina, as seen in Figure 14b.

Different angle-ply lamina were modelled and the mechanical properties were obtained in Table 3. However, there is no specific experiment for these angle-ply lamina, hence the

theoretical and FEM modelling results were used to compare with and validate the DEM model. The comparison between results from the theory, the FEM and the extended 2D hexagonal and square DEM models was conducted and illustrated in Table 3.

Table 3: The comparison of the extended 2D DEM approach against the theoretical and FEM results

	E1 (GPa)	E2 (GPa)	υ_{12}	υ_{21}
30° (Theory)	27.61	15.16	0.567	0.311
30° (FEM)	22.16	15.34	0.41	0.285
30° (DEM)	21.0	15.59	0.466	0.288
45° (Theory)	17.66	17.66	0.515	0.515
45° (FEM)	16.94	16.94	0.386	0.386
45° (DEM)	17.44	17.44	0.475	0.475
60° (Theory)	15.16	27.61	0.311	0.567
60° (FEM)	15.34	22.16	0.285	0.41
60° (DEM)	15.59	21.0	0.288	0.466
90° (Theory)	16.2	45.6	0.0988	0.278
90° (FEM)	16.21	45.71	0.093	0.253
90° (DEM)	15.98	46.03	0.104	0.247

After angle-ply lamina being modelled, the next step is to model the laminate of composites, which requires interface between each ply. The simplest laminate is [0/90/0], which is shown in Figure 15. It is built with three layers, the lower layer and the upper one are 0° ply lamina while the middle one is 90° ply lamina. In this model, the red bonds represent the virtual fibre which has largest normal stiffness, and the light blue bonds represent the matrix while the blue ones represent the interface bonds. Constant velocities are applied on the both sides. The stiffness of the interface bond is hard to determine, so after several attempts with different values, 10^{14} and 10^{13} Pa are adopted for the normal and tangential stiffnesses of the interface bonds, respectively, for the calculation of the Young's Modulus and Poison ratio. After 200, 000 cycles, the results are obtained and shown in Table 4. Good

agreements between theoretical, FEM and DEM results can be observed.

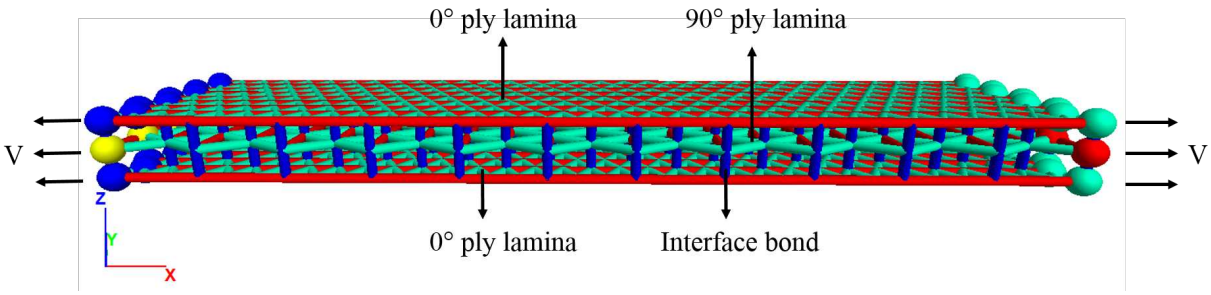

Figure 15: The extended 2D hexagonal DEM model of [0/90/0] laminate

Table 4: Comparison of the DEM, theoretical and FEM results for [0/90/0] cross-ply laminate

	E1 (GPa)	E2 (GPa)	υ_{12}	υ_{21}
theory	36.01	26.15	0.173	0.125
FEM	36.06	26.18	0.161	0.118
DEM	36.12	26.25	0.152	0.116

To further validate the DEM model, a typical example of hole-in-plate under uniaxial tension is studied with displacement distribution compared with a FEM model. The FEM model was modelled with 3D continuum shell element in ABAQUS/Standard. The dimension of the two models is 60 mm × 36 mm × 1.5 mm with a hole of 3 mm. For a fine mesh in the vicinity of the hole, a planar mesh size of 0.318 mm × 0.155 mm was utilized while a coarser mesh was used away from the hole considering the computation. In the FE model, there are 7, 097 shell elements used for the validation, while for the DEM model, 22, 492 balls were used for the comparison. A velocity of 1 mm/s was applied to the both sides. After 0.1 mm displacement, the displacement distributions of the two models are obtained. Figure 16 illustrates the surface displacement distribution of the cross-ply laminates from the two different models, which are matching well. For the displacement distribution, little difference is found.

Finally, an angle-ply composite DE model is also conducted to compare with the FE model and the theoretical results. The FE model was built with continuum shell element

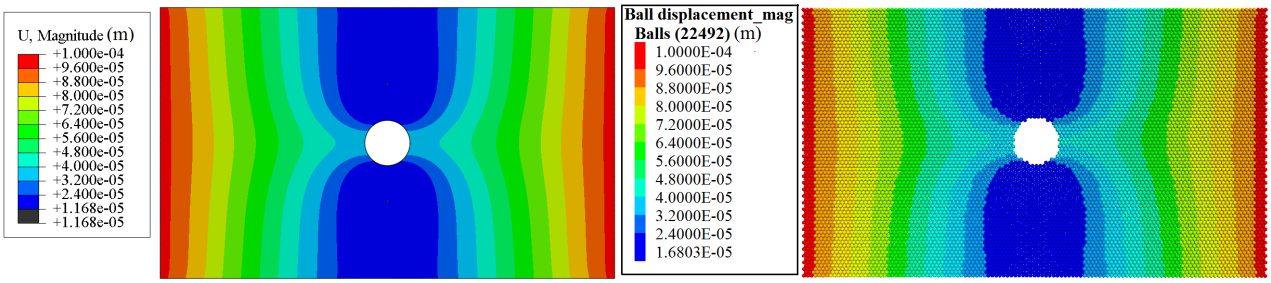

(a) FEM model (b) DEM model

Figure 16: Displacement distribution in DEM and FEM models for the [0/90/0] cross-ply laminate

in ABAQUS/Standard as above to obtain its Young's Moduli and Poisson's ratios. Figure 17 shows the layout of the laminates is $[0/30/45]_s$ and the strength of the interface bonds is set to be very large to maintain elasticity. The velocity of $1mm/s$ is applied to both sides. As listed in Table 5, only little discrepancy is found between DEM, FEM and theoretical results in terms of the Young's Moduli and Poisson's ratios.

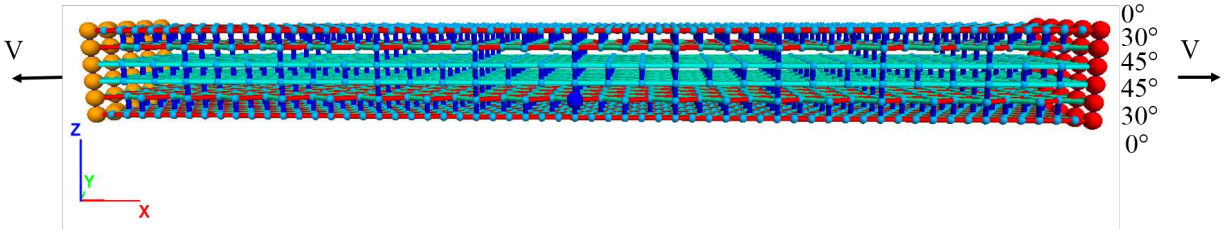

Figure 17: 3D DEM model of $[0/30/45]_s$ angle-ply laminate

Table 5: Elasticity property from theory, FEM and DEM for $[0/30/45]_s$ angle-ply laminate

	E1 (GPa)	E2 (GPa)	υ_{12}	υ_{21}
theory	30.617	17.333	0.464	0.263
FEM	29.49	17.036	0.362	0.214
DEM	29.68	17.01	0.49	0.31

5. Conclusions

In this study, three different DEM packing approaches, have been assessed and evaluated against experimental data, theoretical calculations and FEM results in order to identify the most effective and efficient method for modelling anisotropic fibre reinforced composite laminate. It has been found that the extended 2D hexagonal and square modelling approach is capable of modelling the lamina in any angles as well as cross-ply and angle-ply composite laminates. For the validation of angle-ply lamina and laminates, Classic Composite Laminate Theory and FEM are employed for comparison and validation. A few conclusion are summarized as below:

1. It was found that 3D lattice discrete model is not suitable for modelling of composite lamina/laminates due to the weakness in dealing with particle breakage and poor performance in representing anisotropy. 3D HCP model and extended 2D hexagonal and square model are capable of modelling the composite lamina. However, considering the computation cost, the extended 2D hexagonal model is more efficient.
2. This is the first attempt to model the 0°, 30°, 60° 90° ply composite laminae with hexagonal packing and 45° ply composite lamina with square packing in 3D model. Different anisotropic properties can be achieved by assigning the different stiffnesses to the corresponding directions. The mechanical properties of the extended 2D hexagonal and square model for the angle-ply lamina are in good agreement with the theoretical and FEM results.
3. The extended 2D hexagonal and square model is used to model the cross-ply and angle-ply laminates. The DEM simulated mechanical properties are very close to those from the theory and FEM. The displacement distribution from a plate with a hole are compared with the FE model and the DE model, good agreement has been observed.

In the future, constitutive models will be introduced the developed DEM model to enable bond-breaking so as to simulate the initiation and progressive failure of the composite laminates. In addition, GPU computation can be adopted to facilitate large scale modelling of composite failure based on the current DEM approach.

6. Acknowledgement

The first author would like to thank China Scholarship Council for the financial support.

References

[1] D. Yang, J. Ye, Y. Tan, Y. Sheng, Modeling progressive delamination of laminated composites by discrete element method, Computational Materials Science 50 (3) (2011) 858–864.

[2] Z. Hashin, Fatigue failure criteria for unidirectional fiber composites, ASME, Transactions, Journal of Applied Mechanics 48 (1981) 846–852.

[3] S. W. Tsai, E. M. Wu, A general theory of strength for anisotropic materials, Journal of composite materials 5 (1) (1971) 58–80.

[4] A. Kaddour, M. Hinton, Maturity of 3D failure criteria for fibre-reinforced composites: Comparison between theories and experiments: Part B of WWFE-II, Journal of Composite Materials 47 (6-7) (2013) 925–966.

[5] A. Kaddour, M. Hinton, P. Smith, S. Li, Mechanical properties and details of composite laminates for the test cases used in the third world-wide failure exercise, Journal of Composite Materials 47 (20-21) (2013) 2427–2442.

[6] A. Kaddour, M. Hinton, P. Smith, S. Li, The background to the third world-wide failure exercise, Journal of Composite Materials 47 (20-21) (2013) 2417–2426.

[7] A. Kaddour, M. Hinton, P. Smith, S. Li, A comparison between the predictive capability of matrix cracking, damage and failure criteria for fibre reinforced composite laminates: Part A of the third world-wide failure exercise, Journal of Composite Materials 47 (20-21) (2013) 2749–2779.

[8] A. Scott, M. Mavrogordato, P. Wright, I. Sinclair, S. Spearing, In situ fibre fracture measurement in carbonepoxy laminates using high resolution computed tomography, Composites Science and Technology 71 (12) (2011) 1471–1477.

[9] Q. Yang, D. Schesser, M. Niess, P. Wright, M. Mavrogordato, I. Sinclair, S. Spearing, B. Cox, On crack initiation in notched, cross-plied polymer matrix composites, Journal of the Mechanics and Physics of Solids 78 (Supplement C) (2015) 314–332.

[10] C. McCarthy, M. McCarthy, V. Lawlor, Progressive damage analysis of multi-bolt composite joints with variable bolthole clearances, Composites Part B: Engineering 36 (4) (2005) 290–305.

[11] L. Zhao, N. Warrior, A. Long, Finite element modelling of damage progression in non-crimp fabric reinforced composites, Composites Science and Technology 66 (1) (2006) 36–50.

[12] I. Lapczyk, J. A. Hurtado, Progressive damage modeling in fiber-reinforced materials, Composites Part A: Applied Science and Manufacturing 38 (11) (2007) 2333–2341, compTest 2006.

[13] D. Feng, F. Aymerich, Finite element modelling of damage induced by low-velocity impact on composite laminates, Composite Structures 108 (Supplement C) (2014) 161–171.

[14] C.-S. Lee, J.-H. Kim, S. kee Kim, D.-M. Ryu, J.-M. Lee, Initial and progressive failure analyses for composite laminates using Puck failure criterion and damage-coupled finite element method, Composite Structures 121 (Supplement C) (2015) 406–419.

[15] F. Freddi, M. Savoia, Analysis of FRP-concrete debonding via boundary integral equations, Engineering Fracture Mechanics 75 (6) (2008) 1666–1683.

[16] M. Kamiski, Stochastic Boundary Element METHOD analysis of the interface defects in composite materials, Composite Structures 94 (2) (2012) 394–402.

[17] R. Talreja, C. V. Singh, Damage and failure of composite materials, Cambridge University Press, 2012.

[18] F. París, E. Correa, V. Mantič, Micromechanical Evidences on Interfibre Failure of Composites, in: The Structural Integrity of Carbon Fiber Composites, Springer, 2017, pp. 359–390.

[19] D. Iliescu, D. Gehin, I. Iordanoff, F. Girot, M. Gutirrez, A discrete element method for the simulation of CFRP cutting, Composites Science and Technology 70 (1) (2010) 73–80.

[20] M. J. Swindeman, E. V. Iarve, R. A. Brockman, D. H. Mollenhauer, S. R. Hallett, Strength prediction in open hole composite laminates by using discrete damage modeling, AIAA journal.

[21] Y. Ismail, Y. Sheng, D. Yang, J. Ye, Discrete element modelling of unidirectional fibre-reinforced polymers under transverse tension, Composites Part B: Engineering 73 (2015) 118–125.

[22] Y. Ismail, D. Yang, J. Ye, A DEM model for visualising damage evolution and predicting failure envelope of composite laminae under biaxial loads, Composites Part B: Engineering 102 (2016) 9–28.

[23] R. M. Jones, D. A. Nelson Jr, A new material model for the nonlinear biaxial behavior of ATJ-S graphite, Journal of Composite Materials 9 (1) (1975) 10–27.

[24] J. Crews, K. Shivakumar, I. Raju, Strain energy release rate distributions for double cantilever beam specimens, AIAA J 29 (10) (1991) 1686–1691.

[25] M. Kumar, R. Shenoi, S. Cox, Experimental validation of modal strain energies based damage identification method for a composite sandwich beam, Composites Science and Technology 69 (10) (2009) 1635–1643.

[26] I. Raju, J. Crews, M. Aminpour, Convergence of strain energy release rate components for Edge-Delaminated composite laminates, Engineering Fracture Mechanics 30 (3) (1988) 383–396.

[27] I. Itasca Consulting Group Inc., PFC 5.0 documentation.

[28] L. Trivino, B. Mohanty, Assessment of crack initiation and propagation in rock from explosion-induced stress waves and gas expansion by cross-hole seismometry and FEM-DEM method, International Jour-

nal of Rock Mechanics and Mining Sciences 77 (Supplement C) (2015) 287–299.

[29] M. Nitka, J. Tejchman, Modelling of concrete behaviour in uniaxial compression and tension with dem, Granular Matter 17 (1) (2015) 145–164.

[30] S. Jiang, T. Li, Y. Tan, A dem methodology for simulating the grinding process of sic ceramics, Procedia Engineering 102 (Supplement C) (2015) 1803–1810.

[31] J. Bolander, S. Saito, Fracture analyses using spring networks with random geometry, Engineering Fracture Mechanics 61 (5) (1998) 569–591.

[32] C. T. Davie, N. Bianic, Failure criteria for quasi-brittle materials in lattice-type models, Communications in Numerical Methods in Engineering 19 (9) (2003) 703–713.

[33] M.-B. Liu, G.-R. Liu, Particle methods for multi-scale and multi-physics, World Scientific, 2015.

[34] F. A. Tavarez, M. E. Plesha, Discrete element method for modelling solid and particulate materials, International Journal for Numerical Methods in Engineering 70 (4) (2007) 379–404.

[35] C. Liu, D. D. Pollard, B. Shi, Analytical solutions and numerical tests of elastic and failure behaviors of close-packed lattice for brittle rocks and crystals, Journal of Geophysical Research: Solid Earth 118 (1) (2013) 71–82.

[36] G.-F. Zhao, J. Fang, J. Zhao, A 3D distinct lattice spring model for elasticity and dynamic failure, International Journal for Numerical and Analytical Methods in Geomechanics 35 (8) (2011) 859–885.

[37] C. Liu, Q. Xu, B. Shi, S. Deng, H. Zhu, Mechanical properties and energy conversion of 3D close-packed lattice model for brittle rocks, Computers & Geosciences 103 (2017) 12–20.

[38] Z. P. Bazant, Softening instability: Part I-Localization into a planar band, Journal of applied mechanics 55 (3) (1988) 517–522.

[39] F. C. Caner, Z. P. Bažant, Microplane model M7 for plain concrete. I: Formulation, Journal of Engineering Mechanics 139 (12) (2012) 1714–1723.

[40] Z. P. Bažant, G. Zi, Microplane constitutive model for porous isotropic rocks, International journal for numerical and analytical methods in geomechanics 27 (1) (2003) 25–47.

[41] A. Beghini, Z. P. Bažant, Y. Zhou, O. Gouirand, F. C. Caner, Microplane model M5f for multiaxial behavior and fracture of fiber-reinforced concrete, Journal of engineering mechanics 133 (1) (2007) 66–75.

[42] M. Brocca, Z. P. Baant, I. M. Daniel, Microplane model for stiff foams and finite element analysis of sandwich failure by core indentation, International Journal of Solids and Structures 38 (44) (2001) 8111–8132.

[43] G. Cusatis, A. Beghini, Z. P. Bažant, Spectral stiffness microplane model for quasibrittle composite laminates-Part I: theory, Journal of Applied Mechanics 75 (2) (2008) 021009.

[44] E. Kuhl, G. A. D'Addetta, H. J. Herrmann, E. Ramm, A comparison of discrete granular material

models with continuous microplane formulations, Granular Matter 2 (3) (2000) 113–121.

[45] I. Carol, M. Jirsek, Z. P. Baant, A framework for microplane models at large strain, with application to hyperelasticity, International Journal of Solids and Structures 41 (2) (2004) 511–557.

[46] E. Kuhl, G. A. D'Addetta, M. Leukart, E. Ramm, Microplane modelling and particle modelling of cohesive-frictional materials, Springer Berlin Heidelberg, 2001, pp. 31–46.

[47] V. Šmilauer, Cross-anisotropy model with discrete elements, `https://woodem.org/cases/x-aniso/index.html` (2012).

[48] A. Kaddour, M. Hinton, Input data for test cases used in benchmarking triaxial failure theories of composites, Journal of Composite Materials 46 (19-20) (2012) 2295–2312.

[49] Y. Wang, P. Mora, Macroscopic elastic properties of regular lattices, Journal of the Mechanics and Physics of Solids 56 (12) (2008) 3459–3474.

[50] N. R. Center, Similarities and difference between the fcc and hcp structure, `https://www.nde-ed.org/EducationResources/CommunityCollege/Materials/Structure/fcc_hcp.htm` (2001).

[51] K. Liu, W. Liu, Application of discrete element method for continuum dynamic problems, Archive of Applied Mechanics 76 (3-4) (2006) 229–243.